AIAA AVIATION Forum
June 15-19, 2020, VIRTUAL EVENT
AIAA AVIATION 2020 FORUM

10.2514/6.2020-2532

Sound Production due to Swirl-Nozzle Interaction: Model-Based Analysis of Experiments

L. Hirschberg*
German Aerospace Center, 10623 Berlin, Germany

S. J. Hulshoff†
Delft University of Technology, 2629 HS Delft, the Netherlands.

F. Bake ‡
German Aerospace Center, 10623 Berlin, Germany

Indirect noise due to the interaction of flow inhomogeneities with a choked nozzle is as an important cause of combustion instability in solid rocket motors and is believed to be important in aircraft engines. A previously published experiment demonstrated that interaction of the nozzle with time-dependent axial swirl can also be a source of sound. This axial swirl was generated by intermittent circumferential mass injection upstream from a choked nozzle in a so-called Vortex Wave Generator. The present work discusses the impact of swirl-nozzle interaction in this experiment on the acoustic waves detected downstream of the nozzle. The main source of sound appears to be the reduction in mass flux through the choked nozzle, which depends quadratically on the swirl number. This effect is quantitatively predicted by a quasi-steady and quasi-cylindrical analytical model. The model, combined with empirical data for the decay of axial swirl in pipe flows, predicts the observed influence of the distance between the Vortex Wave Generator and the nozzle. The findings presented here contradict the hypothesis found in the literature, which presumes that sound production in the above-mentioned experiment is due to the acceleration of vorticity waves through the nozzle.

I. Introduction

Vortex-driven indirect-combustion noise is known to play a major role in the establishment of self-sustained pressure pulsations in large Solid Rocket Motors [1–4], and is believed to be an indirect-combustion noise source in aircraft engines [5, 6]. Vortex-driven indirect-combustion noise will partly be radiated outward, thus contributing to environmental noise.

Kings and Bake [5] performed a series of unique experiments with the aim of advancing the fundamental understanding of vortex-nozzle interaction. These experiments were performed using a modified version of the rig used for earlier canonical Entropy Wave Generator experiments [8]. Specifically, the heating module in the Entropy Wave Generator rig was replaced by a Vorticity Wave Generator module (VWG). Kings' and Bake's experiment is described in section II.

Kings and Bake hypothesized that the sound production in the experiments was due to acceleration of vorticity through the nozzle [5]. This hypothesis was inspired by Howe's and Liu's [7] paper, in which a low Mach number theory for the interaction of linear vorticity waves with a duct contraction was developed.

To the best of the authors' knowledge, in the literature there is only one attempt at model-based analysis of the above mentioned experiments, that by Ullrich et al. [6] who reported simulations which used a hybrid CFD/CAA model. Echoing Kings' and Bake's hypothesis, Ullrich's et al. [6] modeling approach fundamentally supposed that sound production in the experiments was due to acceleration of vorticity waves through the nozzle.

In this paper, a radically novel analysis of the Kings' and Bake's experiments [5] is provided. In section II, the experiment is described. In the experiments, temporary circumferential gas injection was added to an axial stationary

*DLR-DAAD Postdoctoral Fellow, German Aerospace Center, Institute of Propulsion Technology, Engine Acoustics, Mueller-Breslau-Straße 8, 10623 Berlin, Germany, AIAA Member.

†Assistant Professor, Faculty of Aerospace Engineering, Delft University of Technology, Kluyverweg 1, 2629 HS Delft, the Netherlands

‡Team Leader Combustion Acoustics, German Aerospace Center, Institute of Propulsion Technology, Engine Acoustics, Mueller-Breslau-Straße 8, 10623 Berlin, Germany, AIAA Member.

base flow upstream from a choked nozzle. The resulting flow is argued to consist of two components. The first of these is a combination of axial and azimuthal flow, here referred to as the swirl component. The second is a vortical structure in a plane normal to the streamline of the swirl component, referred to here as the normal vortex component. As the upstream-generated swirl flow structure moves with the main flow, it interacts with the choked nozzle producing sound. Results, in section III, obtained with a model for the normal vortex component show that its contribution to sound production in the experiments is negligible. In section IV, a quasi-steady model for sound production due to interaction of the swirl component of the flow with the nozzle is presented and favorably compared to the experimental results. The details of the model for the normal vortex component of the generated flow structure can be found in appendix A. Appendix B provides supplemental derivation details concerning the model for interaction of the choked nozzle with the swirl component. In appendix C, it is argued that the normal shock present in the diverging part of the nozzle will, for the given experimental condition, not have a significant influence on the acoustic wave propagation. Contributions to sound production due to reservoir pressure variation and entropy sound are discussed in appendices D and E. Conclusions are summarized in section V.

II. The Vorticity Wave Generator Experiment

In section II.A, the experimental setup used by Kings and Bake [5] is described. After which, in section II.B Kings' and Bake's [5] recorded signal is discussed. Remarks concerning the evolution of the generated flow structure are provided in section II.C.

A. Experimental Setup

In Fig. 1 a schematic sketch of the experimental setup is shown. The upstream part of the setup consisted of an upstream settling chamber (with a volume of 4.6 l) with a bell-mouth inlet to a tube section. The tube had a 15 mm radius and 100 mm length (tube section 1 in Fig. 1). A single Vorticity Wave Generator (VWG) was connected to the downstream end of this tube section. The VWG was followed by a uniform exchangeable tube of radius 15 mm (section 2 in Fig. 1). Tube lengths of 50, 100, and 200 mm could be used, resulting in short, medium and long configurations. After section 2 was a converging-diverging nozzle with throat diameter 7.5 mm. Downstream from the nozzle there was a uniform tube (radius 20 mm and a length of 1020 mm) referred to as the "microphone section." Four microphones (GRAS 40BP 1/4" Ext. Polarized Pressure Microphones) were mounted flush in the wall of this microphone section. These were used to detect pressure waves generated by generated-flow structure-nozzle interaction. An "anechoic" termination* was connected to the microphone section by a flexible tube (radius 20 mm and 980 mm length). The effect of acoustic reflections from this termination is discussed in section II.B.

The VWG consisted of a 70 mm long tube with a 15 mm radius. In the VWG, a small nozzle of outlet radius 1.5 mm was used to circumferential inject gas into a preexisting stationary, non-swirling axial base flow (Fig. 2). This stationary base flow was created by imposing a mass-flow rate of 41 $\mathrm{kg} \cdot \mathrm{h}^{-1}$ upstream from the nozzle. At this mass-flow rate, choked nozzle conditions were obtained. The VWG's circumferential gas injection lasted 0.1 s. For the experimental results analyzed in this text (Fig. 3 subsection II.B), the circumferential injection mass-flow rate was varied between 0.55 $\mathrm{kg} \cdot \mathrm{h}^{-1}$ and 1.10 $\mathrm{kg} \cdot \mathrm{h}^{-1}$. These injection rates correspond to the measured average over 300 1.0 s experiments (obtained using a Bronckhorst F-203AV mass flow controller in the passive setting). In each experiment the fast switching injection valve was held open for 0.1 s. Details about the fast-switching injection valve can be found in Ref. [25]. The opening and closing time of the valve was of the order of 2.5 ms [25].

In Fig. 2, one can see a closed radial injection port. Radial injection does not generate a swirling flow component. Kings used such a radial injection port to study "direct noise" caused by the injection of gas on the preexisting stationary flow [12]. In Ref. [12], Kings shows that when the nozzle is critical, most of the direct noise due to gas injection is reflected back upstream, and only a small part travels downstream through the sonic line. A discussion of some aspects of Kings' radial injection experiments is provided in appendix D.

The convergent divergent nozzle had a surface contraction ratio of $1/16$. Choked, it imposed an upstream nominal inlet Mach number of $M \simeq 3.6 \times 10^{-2}$.

*The termination was found not be completely anechoic in a study of Bake's EWG experiments by Leyko et al. [14]. The termination is not anechoic at very low frequencies.

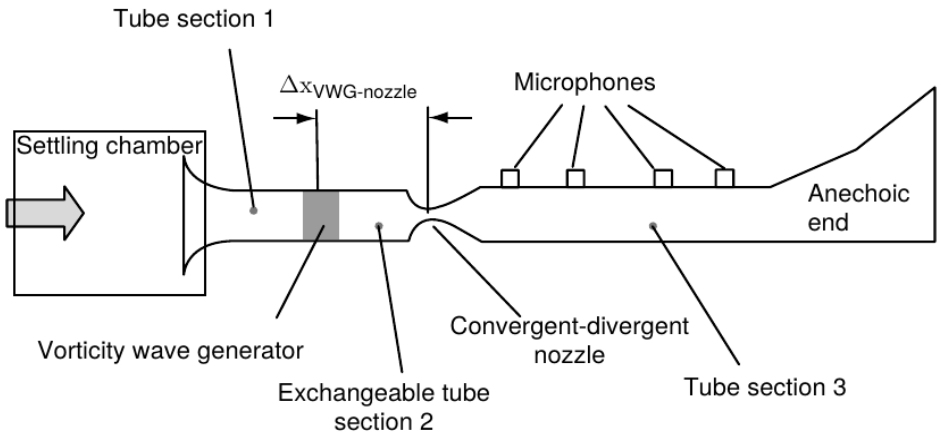

Fig. 1 Schematic sketch of the Vortex Wave Generator experimental setup.

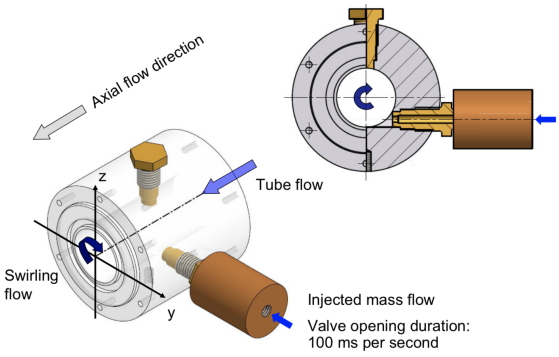

Fig. 2 The Vorticity Wave Generator module (VWG).

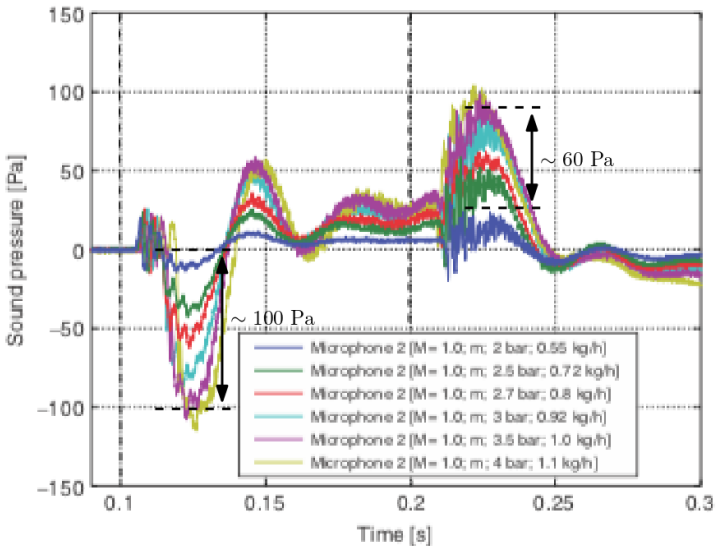

Fig. 3 Downstream recorded pressure signal due to vortex nozzle interaction.

B. Recorded Acoustic Signal

In Fig. 3 the measured pressure signals reported by Kings and Bake [5] are shown. The signals were recorded with the second microphone downstream from the nozzle throat, referred to as microphone 2. The distance between the nozzle throat and microphone 2 was 730 mm. The signals in Fig. 3 were obtained using the medium configuration with six circumferential time-averaged mass injection flow rates between 0.55 kg $\cdot$ h^{-1} and 1.1 kg $\cdot$ h^{-1}. These injection rates correspond to the apparent[†] average over the 300 experiments of 1.0 s each, during which the injection valve was open for 0.1 s (measured using a Bronckhorst F-203AV mass-flow controller in the passive setting).

Fig. 4 shows the influence of a varied section 2 pipe length on the first part of the experimentally-obtained signal. The section 2 pipe lengths are: 50 mm (short configuration, used for the blue line in Fig. 4), 100 mm (medium configuration, used for the results shown in Fig. 3 and red red line in Fig. 4) and 200 mm (long configuration, used for the green line in Fig. 4). Note that the beginning of the strong acoustic pressure peak induced by the entrance of the vortex in the nozzle occurs with a time delay relative to the beginning of the direct sound generated by the unsteady volume injection (at 0.105 s). This can be estimated as the convection time between the injection point and the nozzle inlet. This distance for the three configurations is 85mm, 135 mm and 235 mm, respectively. The main flow velocity of 12.5 m $\cdot$ s^{-1} leads to convective delays of 6.8 ms, 10.8 ms and 18.8 ms. The sound generated by vortex-nozzle interaction should therefore begin at t = 0.112 s, 0.116 s and 0.124 s, respectively. This agrees qualitatively with the experimental results shown in Fig. 4 confirming that the observed negative acoustic peak is due to the arrival of the vortex at the nozzle..

At $t \simeq 0.13$ s one observes a negative acoustic pressure peak difference of 40 Pa between results obtained with the long configuration compared to the short configuration. This difference can be explained by swirl decay in the upstream tube and is expanded upon in sections IV.B and IV.E.

In Figs. 3 and 4, two vertical dashed lines are drawn at 0.1 s and 0.2 s. These correspond to the initiation of electrical signals for the opening and closing of the circumferential mass injection valve, respectively. After the valve is opened, one observes a time delay of ca. 5 ms before an oscillating signal with a frequency of 2×10^2 Hz is observed (for an apparent mass-flow rate of 1.1 kg $\cdot$ h^{-1}).

This first recorded signal is due to a to a quarter-wavelength oscillation, caused by the abrupt start of circumferential mass injection in the pipe section upstream of the nozzle throat (in Figs. 1: tube section 1, VWG, and section 2). This signal is referred to as direct sound, because it does not involve the interaction of the nozzle with the structure generated by circumferential mass injection. For the short, medium and long configurations, section 1, the VWG module

[†]The average injection mass-flow rates were obtained using a Bronckhorst F-203AV mass flow controller in the passive setting. This apparatus is not designed for measurement of fast varying mass flows. Because of this there is a large uncertainty in Kings' and Bake's [5] reported average circumferential mass-flow rate $\dot{m}_\theta$ values.

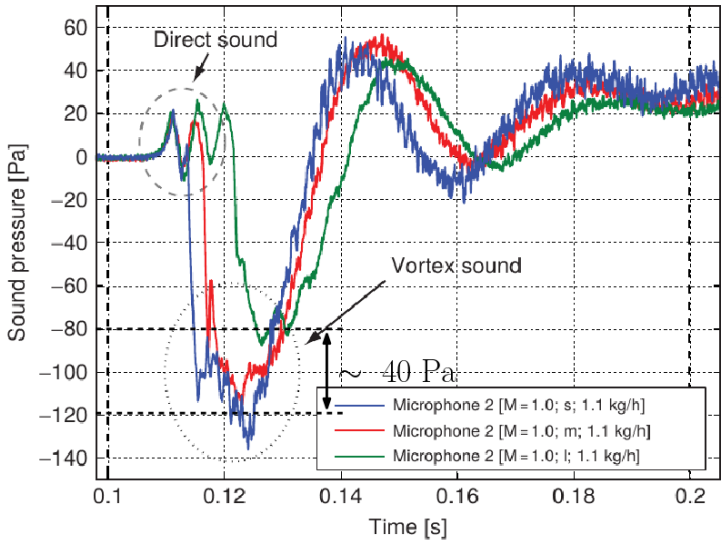

Fig. 4 Influence of section 2 length on acoustic signal, where the blue, red and green lines are for 50 mm**,** 100 mm **and** 200 mm **section lengths, respectively. Figure taken form Ref. [5] and retouched.**

and section 2 have a combined length of 0.220 m, 0.270 m and 0.370 m, respectively. Assuming an end correction for the open side of the tube (at bell-mouth inlet) of 0.03 m, one can estimate the frequency of a quarter-wavelength oscillation in the upstream pipe sections. Using $f_1 = c/(4L_1)$, one estimates quarter-wavelength oscillation frequencies of 3.4×10^2 Hz, 2.8×10^2 Hz and 2.1×10^2 Hz for the short, medium and long configurations, respectively. Essentially, these correspond to what was experimentally observed, viz., using Fig. 4 one estimates for the short, medium and long configurations direct noise quarter-wavelength oscillation frequencies of 3.4×10^2 Hz, 2.6×10^2 Hz and 2.2×10^2 Hz.

The influence of radial injection without swirl is considered in Appendices D and E. In appendix D a model is proposed for the effect of changes in reservoir pressure associated with the additional injection of fluid and changes in mass flux through the nozzle. Appendix E discusses the effect of the entropy non-uniformity of the flow.

After this signal, there is a second lower-frequency (28 Hz) strongly-damped acoustic pressure signal (Fig. 3). This starts with a strong negative peak, related to a decrease of mass flux through the nozzle throat when the generated flow structure enters the nozzle. The following oscillation of 28 Hz corresponds to a strongly damped quarter-wavelength oscillation in the part of the experimental setup downstream from the nozzle throat. It is most pronounced for an apparent circumferential mass injection of 1.1 kg $\cdot$ h^{-1}. With an effective diffusor section length of $0.250/3$ m $\simeq 8 \times 10^{-2}$ m, microphone section length of 1.02 m, flexible tube length of 0.98 m and assuming the termination module to have an acoustic-effective length of 0.92 m, one estimates $f_2 \simeq 340$ m $\cdot$ s$^{-1}/(4 \times 3.0\text{m}) \simeq 28$ Hz. As will be explained in more detail in section IV.C, this signal is triggered by the decrease in mass flux trough the nozzle caused by the presence of the swirl component in the nozzle throat.

After a delay of approximately 5 ms following the electrical signal at 0.2 s driving the closing of circumferential mass injection valve, one again observes a 2.6×10^2 Hz quarter-wavelength oscillation of the upstream pipe section (with respect to the nozzle throat). Superimposed on this 2.6×10^2 Hz oscillation one observes a strong oscillation at about 1 kHz. The 1 kHz is assumed to be due to a quarter-wavelength oscillation in the injection pipe, between the injection orifice and the closed fast valve (corresponding to an effective length of ca. 8 cm). This is followed by a superimposed strongly-damped 28 Hz quarter-wavelength oscillation in the downstream part of the setup. This strongly-damped oscillation starts with an initial positive peak. Its origin is the abrupt increase of mass flux through the nozzle as the swirl component leaves the nozzle. This sound production mechanism will be expanded on in section IV.C.

It is interesting to note that there is some asymmetry between the initial negative pulse observed at 0.13 s, of ca. -100 Pa due to the entrance of the vortex in the nozzle, and the positive pulse at 0.23 s of ca. $+60$ Pa generated as the vortex leaves the nozzle (see Fig. 3 for 1.1 kg $\cdot$ h^{-1} apparent average measured mass-injection rate). Before the valve is opened air in the pipe upstream from the valve in particular the tube section upstream from the Bronckhorst F-203AV linear resistance flow meter is at reservoir pressure (4 bar). When the valve is opened air situated in the tube connecting the valve to the flow meter is injected circumferentially into the axial main flow. This lowers the pressure in the tube

section between the valve and flow meter with respect to the reservoir pressure upstream from the flow meter, because of the flow resistance of the meter. Thus, during the time the valve is opened this pressure driving the circumferential injection mass-flow rate decreases. This causes the observed asymmetry in the acoustic pressure signal between the opening and closing of the valve.

C. Remarks Concerning the Evolution of the Generated Flow Structure

In Kings' and Bake's experiment [5], the circumferential injection mass-flow rate was reported to have been varied between 0.55 $\mathrm{kg \cdot h^{-1}}$ 1.1 $\mathrm{kg \cdot h^{-1}}$. As explained above, one should note that these injection rates correspond to the apparent average over 300 experiments.

In Ref. [5, 12], Particle Image Velocimetry (PIV) measurements of the resulting swirling velocity field are reported. These PIV measurements were carried out by removing all parts of the setup downstream of a 100 mm exchangeable tube section 2 (medium configuration). A permanent mass-flow of 41 $\mathrm{kg \cdot h^{-1}}$ (Ref. [12]) was imposed through the settling chamber, establishing a stationary base flow in the remaining parts of the setup and a free jet exiting tube section 2. Perpendicular to this free jet, at a distance of 137 mm from the circumferential injection outlet [5], a plane-laser sheet was created for the purpose of PIV measurements. Fig. 5 shows results obtained 15 ms after initiation of the circumferential injection for an apparent average circumferential mass-flow injection of 1.1 $\mathrm{kg \cdot h^{-1}}$ (Ref. [5]).

Due to the fact that no external forces are applied on the free jet, circulation and axial momentum are conserved. The circulation obtained from the results shown in Fig. 5 can be assumed to be the same as in tube section 2. By extension, this is taken to imply that near the outlet the flow has the same swirl number one would expect in the normal closed-off configuration. One can, at the very least, conclude that injection of air using the VWG causes an axially swirling flow, the passage of which through the nozzle causes an acoustic signal (Fig. 3).

Note that compared to reservoir conditions with a choked nozzle upstream from tube section 2, in the free jet where the PIV measurement was performed one had atmospheric (lower) pressure. Thus, the measured axial flow velocity in the free jet was about 10 % higher than the velocity upstream from the nozzle in the case of vortex-nozzle interaction experiments.

Assuming an axial velocity of 13 $\mathrm{m \cdot s^{-1}}$ for the PIV measurements (corresponding to the measured axial mass-flux of 41 $\mathrm{kg \cdot h^{-1}}$), one finds that the generated flow structure should be approximately 0.2 m long after 15 ms. Noting that the result shown in Fig. 5 was measured at a distance of 137 mm and 15 ms after the injection valve was opened, one may take the PIV measurements to be a cross-sectional cut perpendicular to the axial flow, across a generated flow structure. Given the velocity vectors and, asymmetry in Fig. 5, viz., the red colored three-quarter circle higher velocity region, one concludes that a helicoidal swirling flow is formed and that the PIV measurements show snapshots as it is convected trough the measurement plane.

One observes that the helical flow structure diverges. Namely, in PIV measurement (Fig. 5) which was taken near the outlet, the high velocity region is farther removed from the center of the jet that the 15 mm radius of the outlet. In the literature this phenomenon is reported in free-jet experiments perturbed by means of steady upstream swirl generation with similar swirl intensities [26, 27] used in the presently analyzed unsteady swirl generation experiments.

Based on what has been discussed above, one can hypothesize that in Kings' and Bake's [5] experiment a structure is generated which has a significant component of axially-oriented vorticity. By virtue of the Helmholtz's 2$^{\mathrm{nd}}$ theorem [9], this structure should be connected to the walls of the test rig (through the viscous boundary layers on the wall). Based on the available data [5] a precise description of the evolution of flow field from the opening to the closing of the valve is not possible. This is especially true near the walls of the experimental setup. However, one should assume that at the beginning and end of the generated flow structure, there will be a vorticity component oriented normal to the wall. Dedicated simulations using a simplified numerical model were used to estimate the order of magnitude of the sound production due to this normal component (section III).

III. Influence of the Normal Vortex Component

In this section, numerical results obtained using a simplified model for the the influence of the normal vortex component of the generated flow structure are briefly discussed. As argued above, by virtue Helmholtz's 2$^{\mathrm{nd}}$ theorem [9], generated flow structure should have such a component at the beginning and end of the vortex, because it must reconnect to the wall of the duct.

To study the contribution of the downstream end (or upstream end) of the normal vortex component to sound production due to nozzle interaction, a quasi two-dimensional model is used. A key aspect of the model is that the cylindrical geometry of the experiment is represented as a rectangular-channel equivalent. Care is taken that the

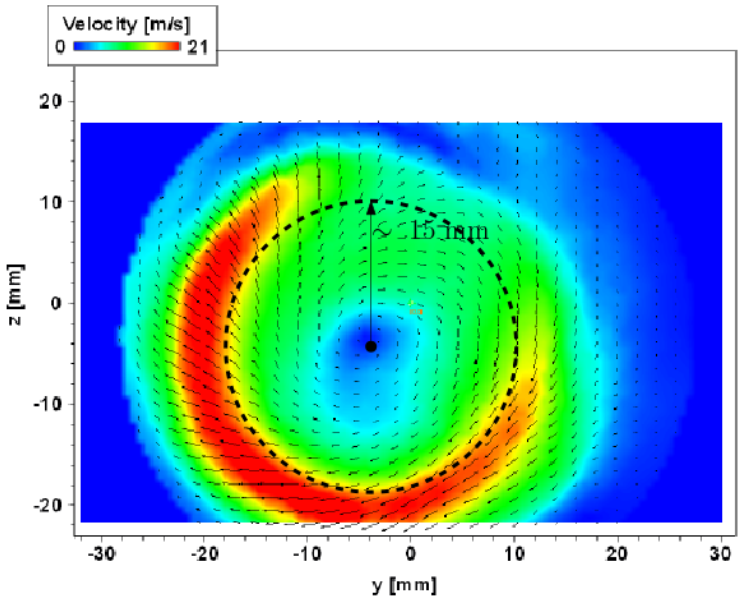

Fig. 5 Image of PIV measurements reported by Kings [12] taken 15 ms **after the trigger for the opening of the circumferential mass injection valve.**

Fig. 6 Scaled image of two-dimensional mesh generated using EIA.

cross-sectional surface areas are maintained, ensuring the same axial evolution of Mach number in choked conditions. The reader is referred to appendix A for details concerning this modeling approach.

Using the above described information (details in A), a two-dimensional mesh was generated. This was done using the Euler Internal Aeroacoustics Code (EIA) internal-mesh generator [4, 10, 11], in Fig. 6 the resulting geometry is shown.

On the generated mesh, a stationary base flow is generated. This is done by imposing soft-pressure-boundary conditions [4] with values of 1.1142×10^5 Pa at the inlet and 1.0090×10^5 Pa at the outlet. These values correspond to the ones in Kings' and Bake's experiments [5].

Using the procedure described in Refs. [4, 11], vortices were generated upstream from the nozzle on the stationary base flow. Vortex generation was initiated at a distance of $3R_\Gamma$ upstream from the nozzle inlet. The resulting vortices travel downstream (along the symmetry axis) with the stationary base flow, and eventually interact with the nozzle, resulting in an upstream-traveling acoustic response. Probes placed upstream from the nozzle were used to record the acoustic signal due to vortex-nozzle interaction.

The circulation of the vortex was chosen to match the circulation observed in the PIV measurement shown in Fig. 5. In Fig. 7, results of vortex-nozzle interaction simulations are shown. Except for the circulation Γ, $\Gamma = 0.6\ \mathrm{m}^2 \cdot \mathrm{s}^{-1}$ (dashed line) and $\Gamma = -0.6\ \mathrm{m}^2 \cdot \mathrm{s}^{-1}$ (solid line), all parameters were kept identical for the displayed results. The viscous vortex-core radius used was $R_\Gamma = 12$ mm for the results shown in Fig. 7. One finds that the acoustic response due to vortex-nozzle interaction is independent of the sign of the circulation Γ, which one expects due to symmetry considerations. The upstream traveling acoustic response is a negative pressure peak. Considering that vortex-nozzle interaction is a dipolar sound source [4, 11], one concludes that an associated positive pressure peak should travel downstream. This is not in agreement with the empirical findings of Kings and Bake [5], which display a negative acoustic peak as the generated flow structure enters the nozzle and a positive peak as the generated flow structure

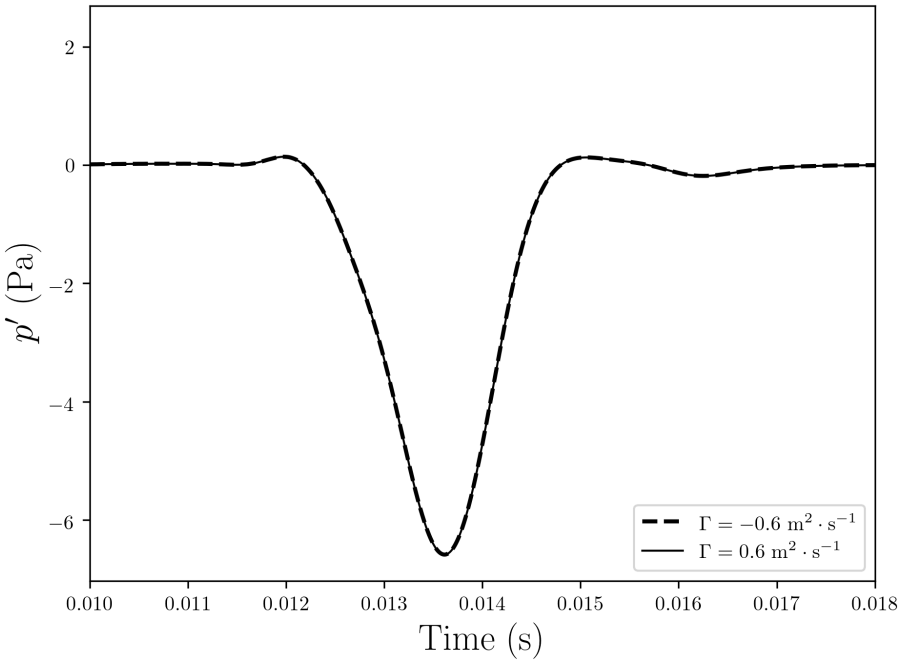

Fig. 7 Upstream-traveling-acoustic response due to vortex-nozzle interaction, for a vortex generated on the symmetry axis.

leaves the nozzle. see Figs. 3 and 4. Furthermore, note that the magnitude (6 Pa) of the predicted upstream pressure pulse is much smaller than that the pressure pulse observed downstream (−100 Pa). Furthermore, note that presented two-dimensional planar model assumes a vortex structure with normal vorticity all across the nozzle cross-section. This should provide an upper-bound for the sound production because the actual normal vorticity structure would join the wall to the the center of the duct. Thus, based on these findings, one concludes that the down and upstream ends of the swirling structure do not account for the experimentally-observed acoustic signal.

IV. Contribution of the Swirl Component

In section IV.A, first a derivation of a simple relation for the nominal swirl, S_N, is derived. The influence of viscous swirl decay as a swirl component is convected through a pipe is described in section IV.B. An analytical model for the quasi-steady response of a choked nozzle to a fluctuation in swirl component is provided in section IV.C. Data from the literature for the response of a choked nozzle steady swirl is discussed in section IV.D. In section IV.E, a model for the acoustic pressure pulse, p'_2, generated in the section downstream from the nozzle is formulated. In the same section two validation strategies are executed.

A. Nominal Swirl

In this section, the definition of the swirl number found in Ref. [13], is used to derive a simple relation for the nominal swirl, S_N, at the circumferential injection position.

Defining the tangential-injector exit surface area $A_\theta \equiv \pi R_\theta^2$ and the cross-sectional surface area of the upstream pipe section $A_1 \equiv \pi R_1^2$, and assuming [22] $(u_\theta/c)^2 << 1$, one has

$$S_N = \frac{\iint_{A_\theta} \rho_\theta R_1 u_\theta^2 \mathrm{d}^2 x}{R_1 \iint_{A_1} \rho_1 u_{\mathrm{ax}}^2 \mathrm{d}^2 x} \tag{1}$$

$$\simeq \left(\frac{\dot{m}_\theta}{\dot{m}_1}\frac{R_1}{R_\theta}\right)^2 \tag{2}$$

where ρ_1 is the gas density in the axial main flow and ρ_θ the density in the injected flow. To find Eq. (2), $\rho_\theta \simeq \rho_1$ is assumed.

For known mass injection rates and geometry of the VWG, the nominal swirl S_N is an estimate for the maximum of the swirl upstream from the nozzle S_1. Which correcting for viscous swirl decay (section IV.B) one could use to predict the acoustic pressure pulse, p_2', generated in the section downstream from the nozzle.

However, in Kings' and Bake's experiments [5] the reported circumferential injection mass-flow rate, $\dot{m}_\theta$, was an apparent average over 300 1.0 s experiments. In each experiment the fast switching injection valve was held open for only 0.1 s. These apparent average injection mass-flow rates were obtained using a Bronckhorst F-203AV mass flow controller in the passive setting. This apparatus is not designed for measurement of fast varying mass flows. Because of this there is a large uncertainty in Kings' and Bake's [5] reported average circumferential mass-flow rate $\dot{m}_\theta$ values. Thus, based on the available data [5] one cannot determine S_N with sufficient precision to warrant its use as an estimate for the maximum value of S_1.

Again, had $\dot{m}_\theta$ been determined more accurately, one would have been able to apply the viscous swirl decay correction described in section IV.B, and use the resulting value of S_1 to predict p_2' using the model presented in section IV.E.

B. Viscous Swirl Decay

Steenbergen and Voskamp [24] describe the decay of swirl in a pipe flow as a process caused by the transport of angular momentum to the pipe wall, viz., viscous action. The process was found to depend on the Reynolds number, Re. The Reynolds number in the upstream pipe section of Kings' and Bake's experiment [5, 12], is estimated as follows:

$$Re_1 = \frac{\rho_1 u_{\mathrm{ax}}(2R_1)}{\mu} \simeq 2.7 \times 10^4.$$

where μ is the dynamic viscosity of the flow.

Following Ref. [24], for a Reynolds of the order estimated above, a simple relation for the swirl, S_1, in the upstream section at a distance Δx in the stream-wise direction from the injection point is proposed:

$$S_1(\Delta x) = S_N \exp\left(-\beta \frac{\Delta x}{2R_1}\right) \tag{3}$$

where the exponential swirl decay rate β is

$$\beta \simeq 0.03.$$

Thus, for a 50 mm pipe length of section 2, at the nozzle inlet (Δx = 85 mm) one finds a swirl reduction factor with respect to the nominal swirl S_N of 0.92. For a section 2 length of 200 mm one finds a swirl reduction factor with respect to S_N of 0.75 (i.e. addition of a 150 mm pipe to section 2 causes a swirl reduction of 0.82 relative to the initial (shorter) configuration). This information will be used later to explain the results shown in Fig. 4.

C. Analytical Model for Quasi-Steady Response of a Choked Nozzle to a Fluctuation in the Swirl Component

In this section, for given fixed reservoir conditions of pressure p_r and temperature T_r, an analytical model for the influence of swirl component on the steady-mass flow through a choked nozzle is presented. The approach described by Gany et al. [13] and van Holten et al. [15] is followed, and a detailed derivation is provided in Appendix B.

The circular cross-section of the nozzle at axial position x is denoted $A(x)$. The nozzle throat corresponding to the minimum of cross-section ($\mathrm{d}A/\mathrm{d}x = 0$) is A_{th}. The hypothetical quasi-one-dimensional isentropic irrotational mass flux, $\dot{m}^*$, through a choked nozzle is given by:

$$\dot{m}^* = \rho^* u^* A_{\text{th}}. \tag{4}$$

Here the critical velocity, u^*, is equal to the critical speed of sound, c^*. For an isentropic flow of an ideal gas with constant specific heat ratio $\gamma = c_p/c_v$ (c_p and c_v at constant pressure and volume respectively), one thus has

$$u^* = c^* = \sqrt{\gamma R T^*} \tag{5}$$

where $R = c_p - c_v$ is the specific ideal gas constant and T^* the critical temperature. T^* is related to the reservoir temperature T_r through Bernoulli's equation [16, 23], as follows

$$T^* = \frac{2}{\gamma + 1} T_r. \tag{6}$$

Due to the axial rotation of the flow, the mass flux through the nozzle will be lower than m^*. To account for this, it is assumed that entropy production during the generation of the swirl component is negligible (see appendix E). Furthermore, it is assumed that the total enthalpy of the flow remains constant and equal to the reservoir enthalpy. And, it is assumed that the flow can be described as quasi one-dimensional, neglecting the non-uniformity induced by the change in cross-section. Gany et al. [13], refer to this approximation as a "quasi-cylindrical" flow and attribute it to Gillespie and Shearer [17]. In this approximation the Mach number at the throat, M_{th}, is related to the local axial velocity, u_{ax}, and local circumferential velocity, u_θ, as follows

$$M_{\text{th}}^2 = 1 + \frac{u_\theta^2}{c_{\text{th}}^2}. \tag{7}$$

Using this result, the stationary mass flux $\dot{m}_{\text{st}} = \dot{m}_{\text{th}}$ (by conservation of mass) can be calculated for an isentropic flow as follows:

$$\dot{m}_{\text{st}} \simeq \rho^* c^* \left(1 - \frac{1}{2}\left(\frac{(u_\theta)_{\text{th}}}{c_{\text{th}}}\right)^2\right) A_{\text{th}} \tag{8}$$

where it is assumed that $(u_\theta/c_{\text{th}})^2 << 1$. Using Eq. (8), one can find an approximation for the quasi-steady relative mass-flux reduction $(\dot{m}_{\text{st}} - \dot{m}^*)/\dot{m}^* \equiv \delta\dot{m}_{\text{st}}/\dot{m}^*$:

$$\frac{\delta\dot{m}_{\text{st}}}{\dot{m}^*} \simeq -\frac{1}{2}\left(\frac{(u_\theta)_{\text{th}}}{c_{\text{th}}}\right)^2. \tag{9}$$

Assuming a uniform circumferential velocity, u_θ, unifrom axial velocity, u_{ax}, and uniform density ρ, the swirl number (Eq. (1)) defined by Gany et al. [13], becomes

$$S = \frac{2u_\theta}{3u_{\text{ax}}}. \tag{10}$$

Solving for u_θ/u_{ax}, one finds

$$\frac{u_\theta}{u_{\text{ax}}} = \frac{3}{2} S \tag{11}$$

Eq. (9), becomes

$$\frac{\delta\dot{m}_{\text{st}}}{\dot{m}^*} \simeq -\frac{9}{8} S_{\text{th}}^2. \tag{12}$$

In section IV.D, this result is compared to empirical data for stationary flow found in the literature.

In the upstream section with cross-sectional surface A_1, one finds, in terms of $(u_\theta)_1$ at A_1, using the conservation of angular momentum assuming a low upstream Mach number $M_1 << 1$, that after some algebra Eq. (12) becomes

$$\frac{\delta\dot{m}_{\text{st}}}{\dot{m}^*} = -\frac{9}{8} S_1^2 \frac{A_{\text{th}}}{A_1} \left(\frac{2}{\gamma + 1}\right)^{\frac{2}{\gamma - 1}} \tag{13}$$

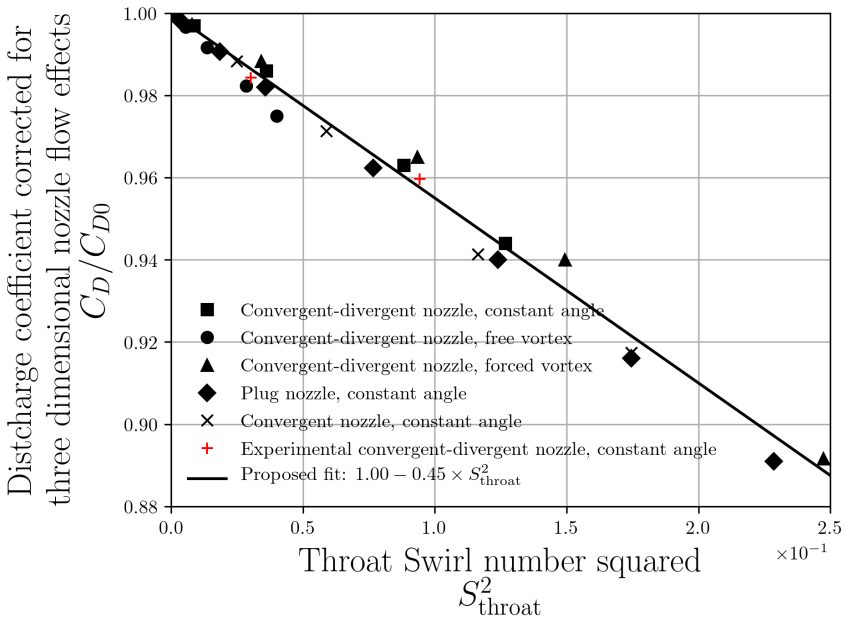

Fig. 8 Simulations (points in black) and measurments (points in red) of C_D/C_{D0} reported by Dutton [20] with proposed modified fit of empirical data.

D. Steady Response of a Choked Nozzle to Variation in Swirl: Available Numerical Simulations and Empirical Data

Experimental results found in the literature [19–21], are presented in terms of the discharge coefficient C_D, defined as

$$C_D \equiv \frac{\dot{m}_{\text{st}}}{\dot{m}^*} \tag{14}$$

which in terms of $\delta\dot{m}_{\text{st}} \equiv \dot{m}_{\text{st}}/\dot{m}^*$, is

$$C_D = 1 + \frac{\delta\dot{m}_{\text{st}}}{\dot{m}^*}. \tag{15}$$

Dutton [19] remarks: “quasi-one-dimensional assumptions are not generally valid since nozzle geometrical constraints often result in highly nonuniform flow field." In practice this leads to the discharge coefficient not reaching the value one. This is clearly visible in the measurements reported by Yoo et al. [21] (Figs. 9, 10, 11 and 12 in Ref. [21]) which demonstrate that the measured C_D will remain about 0.7 % lower than one, even for zero swirl conditions. Accounting for this, Dutton [20] shows results in terms of C_D/C_{D0}, which equals one when $S_{\text{th}} = 0$. In Fig. 8, empirical and numerical data reported by Dutton [20] are shown. Dutton [20] proposed the following least squares fit of the data:

$$\frac{C_D}{C_{D0}} = 1.0 - 0.50526 \times 10^{-2}\,(S_{\text{th}}) - 0.45324\left(S^2_{\text{th}}\right).$$

Because theory (section IV.C) does not predict a linear dependence on the swirl number, an alternative fit which only retains the quadratic term is proposed:

$$\frac{C_D}{C_{D0}} = 1.0 - 0.45 \times S^2_{\text{th}}. \tag{16}$$

As can be seen in Fig. 8, this produces satisfactory agreement with Dutton’s data [20]. Note that Dutton’s results [20] agree with Yoo’s et al. independently obtained experimental results [21].

The analytically-derived model (Eq. (12) in section IV.C), in terms of discharge coefficient, is

$$\frac{C_D}{C_{D0}} = 1 - \frac{9}{8} S_{\text{th}}^2. \tag{17}$$

The second term in this expression differs by a factor 0.40 from the proposed fit (Eq. 16). As pointed out by Dutton [20] and Gany et al. [13], it is noteworthy that when expressed in terms of the swirl number S, the results are insensitive to the distribution of u_θ. Hence, the assumed uniform circumferential velocity is not the cause of this difference between the analytical model and the results of Dutton [20].

E. Comparison to Acoustic Measurements

The variation in mass-flow rate, $\delta\dot{m}/\dot{m}^*$, caused by the swirl component entering (after a small convective time delay with respect to the valve opening) and exiting the nozzle (after the small convective time delay with respect to the valve closing), will induce an expansion and compression acoustic wave downstream. Neglecting the influence of the normal shock in the divergent part of the nozzle (Appendix C), and assuming an infinitely long downstream pipe of uniform cross-section A_2, for the acoustical perturbation u_2' of the axial velocity downstream of the nozzle, one has

$$\frac{u_2'}{u_2} = \frac{\delta\dot{m}}{\dot{m}^*}. \tag{18}$$

where

$$\frac{\delta\dot{m}}{\dot{m}^*} = \begin{cases} +\frac{\delta\dot{m}_{\text{st}}}{\dot{m}^*} \text{ after the valve is opened} \\ -\frac{\delta\dot{m}_{\text{st}}}{\dot{m}^*} \text{ after the valve is closed.} \end{cases} \tag{19}$$

One can estimate the acoustic pressure pulse, p_2', generated in the section downstream from the nozzle, as follows

$$p_2' \simeq \rho_2 c_2 u_2'. \tag{20}$$

Had $\dot{m}_\theta$ been determined more accurately, one would have been able to estimate S_1 and using Eq. 20 determine u_2' for Eq. 18. As explained in section IV.A, one cannot do this with satisfactory accuracy using the available data [5].

Thus, as a means of validation, in the following part of this section this model will be used to determine from the acoustic measurement of p_2' the upstream swirl number, S_1. Using the resulting S_1 estimate the circumferential velocity component, u_θ, will be estimated. This estimation will then compared to Particle Image Velocity (PIV) data reported by Kings and Bake [5]. After this, a second means of validation based on quantifiable viscous decay effects observed in acoustic measurements of p_2' will be provided.

Using Eq. (18), conservation of mass and Eq. (20), one finds

$$\frac{\delta\dot{m}}{\dot{m}^*} = \frac{p_2' A_2}{c_2 \dot{m}_1}. \tag{21}$$

From Fig. 3, one has for an apparent $\dot{m}_\theta = 1.1 \text{ kg} \cdot \text{h}^{-1}$:

$$p_2' \simeq \begin{cases} -100 \text{ Pa after the valve is opened} \\ 60 \text{ Pa after the valve is closed.} \end{cases}$$

Taking these acoustic amplitudes and using Eq. (13), one finds the following estimates for the upstream swirl number:

$$S_1 \simeq \begin{cases} 0.93 \text{ after the valve is opened} \\ 0.72 \text{ just before the valve is closed} \end{cases}$$

which have been corrected for swirl decay (see section IV.B). Estimating the axial velocity, u_{ax}, of the PIV experiment estimated as follows

$$u_{\text{ax}} = \frac{\dot{m}_1}{\rho_2 \pi R_1^2}$$

where

$$\rho_2 = \frac{p_2}{RT_2}$$

is the density in the free jet. Using $p_2 = 1.009 \times 10^5$ Pa, $R = 287.058$ J $\cdot$ kg^{-1} $\cdot$ K^{-1} and $T_2 = 293$ K, one finds for the PIV experiment

$$u_{\mathrm{ax}} \simeq 13 \text{ m} \cdot \text{s}^{-1}.$$

Note that as the structure is formed within 0.1 s (the injection time span), one estimates the swirling component to be about 1.3 m long. I.e. the swirling flow structure is significantly longer than the nozzle. This justifies the quasi-steady approach used for the proposed model.

Using Eq. (11) and $u_{\mathrm{ax}} = 13$ m $\cdot$ s^{-1}, one can estimate the (assumed uniform) circumferential velocity u_θ, as

$$u_\theta = \frac{3}{2} u_{\mathrm{ax}} S_1 \simeq \begin{cases} 18 \text{ m} \cdot \text{s}^{-1} \text{ after the valve is opened} \\ 14 \text{ m} \cdot \text{s}^{-1} \text{ just before valve is closed.} \end{cases}$$

These values appear to be reasonable when compared to the PIV measurements shown in Fig. 5.

Basing the estimation of the upstream swirl number, S_1, on the proposed fit of Dutton's data (Eq. (16)), and correcting for swirl decay, one finds

$$S_1 \simeq \begin{cases} 1.48 \text{ after the valve is opened} \\ 1.13 \text{ just before the valve is closed.} \end{cases}$$

Using these values of S_1 and $u_{\mathrm{ax}} = 13$ m $\cdot$ s^{-1}, the estimation of the circumferential velocity u_θ, yields

$$u_\theta \simeq \begin{cases} 28 \text{ m} \cdot \text{s}^{-1} \text{ after the valve is opened} \\ 22 \text{ m} \cdot \text{s}^{-1} \text{ just before the valve is closed.} \end{cases}$$

One thus finds the correct order of magnitude, both with the above proposed theoretical model and the fit of the Dutton's [20] stationary flow data. However, the estimations based on the fit of Dutton's data (Eq. (16)) do not compare as well as the estimations obtained using the analytical model (Eq. (13)).

Consider Fig. 4, in which the influence of section 2 length variation on the acoustic signal is shown. One observes a decrease of ca. 40 Pa between a 50 mm (blue line) and 200 mm (green line) section 2 tube length. By virtue of Eq. (20) and the theoretical model developed in section IV.C, one knows that

$$p_2' \propto S_1^2. \tag{22}$$

As was discussed in section IV.B, for a section 2 length difference of 150 mm between short and long section 2 configurations (the blue and green lines, respectively) one estimates a relative swirl decay of 0.82. Using this value and Eq. (22), one finds an estimate of 33% for the acoustic pressure signal change due to swirl decay. The negative peak for the shortest configuration has a depth of 120 Pa, which corresponds (by-and-large) to the experimentally-observed 40 Pa acoustic pressure decrease (Fig. 4). This confirms the quadratic dependence of the mass flow reduction on the swirl number and the validity of a quasi-stationary model.

V. Conclusions

In Kings' and Bake's Vorticity Wave Generator experiments [5], a swirling flow structure is generated by periodical circumferential injection of short time duration (0.1 s) in a pipe section upstream of a choked convergent-divergent nozzle. By virtue of Helmholtz's second theorem [9], it has been postulated that this generated flow structure has two components: a principal one which is orientated in the axial direction called the swirl component (characterized by the so-called swirl number), and a normal vortex component at the downstream and upstream ends of the generated flow structure. The latter should have the same circulation as the swirl flow. The contribution of these two components has been modeled separately in this work.

The most important contribution to the recorded signal is due to the passage of the swirl component (ca. 1.3 m long) of the upstream-generated structure. As it transits through the nozzle, it temporarily reduces the mass flux through the nozzle throat. A quasi-steady analytical model of this effect, which includes a model for viscous swirl decay to

predict the influence of the distance between the VWG and the choked nozzle inlet, was used to explain the difference between the short and long upstream channel configurations in the experiments reported by Kings and Bake [5]. The model was used to estimate the circumferential velocity component generated due to circumferential air injection and compared favorably to Particle Velocimetry (PIV) measurements reported by Kings [5]. The model predicts an essentially quadratic swirl number dependence of the generated sound amplitude. This is verified by the unsteady experimental results of Kings and Bake [5] and the steady experiments of Dutton [20] and Yoo et al. [21]. However, the steady experiments of Dutton [20] and Yoo et al. [21] and numerical results of Dutton [20] predict a 2.5 times lower reduction of the mass flow through the nozzle as the analytical model of Gany et al. [13] and van Holten et al. [15]used here.

To investigate the contribution of the downstream and upstream ends of the generated flow structure to the experimentally obtained acoustical signal, a simplified numerical model was developed. The model considered a two-dimensional planar frictionless flow with vorticity normal to the main flow. Sound production due to the down and upstream ends of the swirling flow structure was modeled in a manner similar to the vortex-nozzle interaction simulation reported in Refs. [4, 10]. By virtue of symmetry considerations, the acoustical signal must be independent of the sign of vortex circulation, which has been confirmed. The model predicts a positive pressure pulse generated by the normal vortex component. Considering that, and noting the experimentally recorded acoustic signal begins with a negative peak, continues with a strongly damped oscillation, and ends with an inverted peak and associated damped oscillation, one concludes that the normal vortex component of the generated flow structure does not contribute in first order to the acoustical signal recorded in Kings' and Bake's [5] experiments. Furthermore, the presently presented two-dimensional planar model indicates that the sound pulse generated by normal vorticity is more than an order of magnitude smaller than the observed acoustical signal.

Kings carried out additional radial injection experiments [12], in which no swirl component was generated. These demonstrate that the sound produced by means of radial injection is negligible compared to the sound produced by the interaction of a swirling flow structure with nozzle (see the discussion in appendices D and E). For the case of radial injection, reservoir pressure variation effects have been demonstrated to be significant. The effect of entropy sound has also been estimated (appendix E) but appears to be negligible compared to swirling-flow structure-nozzle interaction.

Appendix

A. Simplified-Numerical Model for Vortex-Nozzle Interaction of Downstream or Upstream Part of the Swirling Flow Structure

To study the contribution of the downstream end (or upstream end) of the swirling flow structure to sound production due to nozzle interaction, a quasi two-dimensional model is proposed. A key aspect of the model is that the cylindrical geometry of the experiment (Fig. 9(a)) is represented as a rectangular-channel equivalent, for which care is taken that the cross-sectional-surface areas are maintained. This ensures the same evolution of Mach number in choked conditions. Thus, in the upstream section of the square channel equivalent has sides $D_1 = \sqrt{\pi} R_1$ and throat $D_{\text{th}} = \sqrt{\pi} R_{\text{th}}^2 / R_1$ dimensions, where $R_1 = 15.0$ mm and $R_{\text{th}} = 3.75$ mm are the experimental tube radii. In the experiment, the nozzle is flush with upstream tube wall. The radius, r, from the center line to the nozzle wall, is

$$r = R_1 + \Delta h - R \sin \phi \tag{23}$$

where $\Delta h = 1.75$ mm, $R = 13$ mm and $\phi \in [\arcsin(\Delta h / R), \pi/2]$, and half the equivalent length, $D/2$, used to describe the nozzle inlet geometry (Fig. 10) for the proposed model is

$$\frac{D}{2} = \frac{\sqrt{\pi}}{2} \frac{r^2}{R_1}. \tag{24}$$

B. Analytical Model for Quasi-Steady Response of a Choked Nozzle to the Swirl Component: Derivation Details

In the "quasi-cylindrical" flow approximation the local Mach number M at a specific point in the flow is related to the local axial velocity, u_{ax}, and local circumferential velocity, u_θ, through the definition

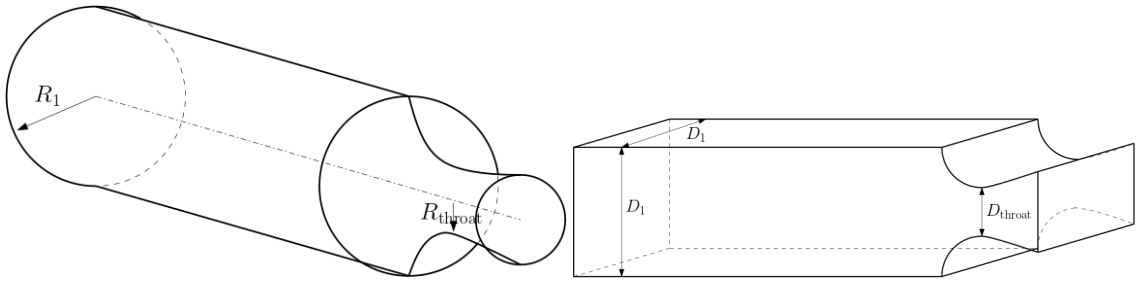

(a) Cylindrical geometry of the experiment (b) Channel equivalent

Fig. 9 (a) Sketch of cylindrically-symmetric geometry. (b) Rectangular equivalent geometry, respecting the evolution of the Mach number.

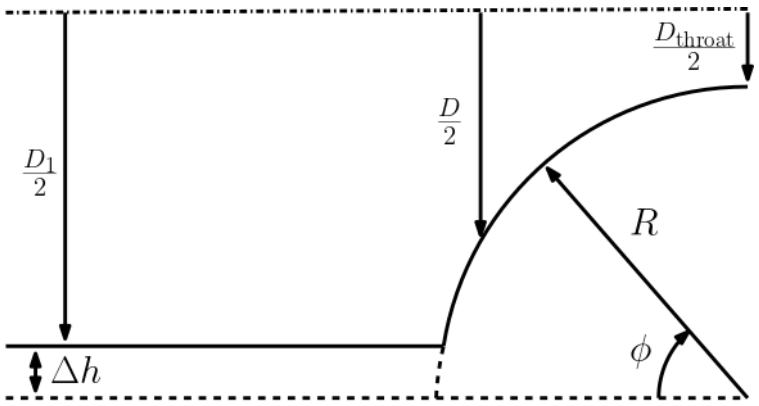

Fig. 10 Definition of square equivalent channel quantities. Where the dashed dotted line is a symmetry line.

$$M^2 = \frac{u_{\mathrm{ax}}^2 + u_\theta^2}{c^2}. \tag{25}$$

The local speed of sound c is related to the reservoir value c_r through Bernoulli's equation, as follows

$$c_r^2 = c^2 + \frac{\gamma - 1}{2}\left(u_{\mathrm{ax}}^2 + u_\theta^2\right). \tag{26}$$

Substitution of Eq. (26) into Eq. (25), yields

$$M^2 = \frac{u_{\mathrm{ax}}^2 + u_\theta^2}{c_r^2 - \frac{\gamma-1}{2}\left(u_{\mathrm{ax}}^2 + u_\theta^2\right)} \tag{27}$$

Furthermore for simplicity, it is assumed that the circumferential velocity u_θ is uniform in each cross-section. This corresponds to Gany et al.'s model [13] (for $n = 0$) and van Holten et al.'s [15] model.

These equations are complemented by the integral-mass-conservation law for the stationary mass flux $\dot{m}_{\mathrm{st}}$:

$$\dot{m}_{\mathrm{st}} = \rho u_{\mathrm{ax}} A = \text{constant} \tag{28}$$

or in differential form

$$\begin{aligned} \frac{1}{\dot{m}_{\mathrm{st}}}\frac{\mathrm{d}\dot{m}_{\mathrm{st}}}{\mathrm{d}x} &= \\ \frac{1}{\rho}\frac{\mathrm{d}\rho}{\mathrm{d}x} + \frac{1}{u_{\mathrm{ax}}}\frac{\mathrm{d}u_{\mathrm{ax}}}{\mathrm{d}x} + \frac{1}{A}\frac{\mathrm{d}A}{\mathrm{d}x} &= 0. \end{aligned} \tag{29}$$

From axial conservation of angular momentum, for a circular cross-section, one has

$$\dot{m}_{\mathrm{st}} u_\theta \sqrt{\frac{A}{\pi}} = \text{constant} \tag{30}$$

or in differential form

$$\begin{aligned} \frac{1}{\dot{m}_{\mathrm{st}}}\frac{\mathrm{d}\dot{m}_{\mathrm{st}}}{\mathrm{d}x} + \frac{1}{u_\theta}\frac{\mathrm{d}u_\theta}{\mathrm{d}x} + \frac{1}{2A}\frac{\mathrm{d}A}{\mathrm{d}x} &= \\ \frac{1}{u_\theta}\frac{\mathrm{d}u_\theta}{\mathrm{d}x} + \frac{1}{2A}\frac{\mathrm{d}A}{\mathrm{d}x} &= 0. \end{aligned} \tag{31}$$

At the throat of the nozzle, where $(\mathrm{d}A/\mathrm{d}x)_{\mathrm{th}} = 0$, using Eq. (31) one finds that

$$\left(\frac{\mathrm{d}u_\theta}{\mathrm{d}x}\right)_{\mathrm{th}} = 0. \tag{32}$$

In the throat, the mass conservation law can then be rewritten, as

$$-\frac{1}{A}\frac{\mathrm{d}A}{\mathrm{d}x} = \frac{1}{\rho}\frac{\mathrm{d}\rho}{\mathrm{d}x} + \frac{1}{u_{\mathrm{ax}}}\frac{\mathrm{d}u_{\mathrm{ax}}}{\mathrm{d}x} = 0 \tag{33}$$

or, using Eq. (32)

$$\frac{1}{\rho}\frac{\mathrm{d}\rho}{\mathrm{d}M^2}\left(\frac{\partial M^2}{\partial u_{\mathrm{ax}}}\frac{\mathrm{d}u_{\mathrm{ax}}}{\mathrm{d}x}\right) + \frac{1}{u_{\mathrm{ax}}}\frac{\mathrm{d}u_{\mathrm{ax}}}{\mathrm{d}x} = 0 \tag{34}$$

where

$$\frac{\partial M^2}{\partial u_{\mathrm{ax}}} = 2\frac{u_{\mathrm{ax}}.c_r^2}{c^4} \tag{35}$$

As the flow is assumed isentropic and the gas ideal, one finds

$$\frac{1}{\rho}\frac{\mathrm{d}\rho}{\mathrm{d}M^2} = -\frac{1}{2}\left(\frac{c}{c_r}\right)^2. \tag{36}$$

.

Substitution of Eqs. (35) and (36) into Eq. (34), because for a choked nozzle $(\mathrm{d}u_{\mathrm{ax}}/\mathrm{d}x)_{\mathrm{th}} \neq 0$, yields

$$(u_{\mathrm{ax}})_{\mathrm{th}} = c_{\mathrm{th}}. \tag{37}$$

Consequently, the Mach number at the throat is

$$M_{\mathrm{th}}^2 = 1 + \frac{u_\theta^2}{c_{\mathrm{th}}^2}. \tag{38}$$

Using this result, the stationary mass flux $\dot{m}_{\mathrm{st}} = \dot{m}_{\mathrm{th}}$ (conservation of mass) can be calculated for an isentropic flow, as follows

$$\begin{aligned} \dot{m}_{\mathrm{st}} &= \rho_{\mathrm{th}}\,(u_{\mathrm{ax}})_{\mathrm{th}}\,A_{\mathrm{th}} \\ &\simeq \rho^* c^* \left(1 - \frac{1}{2}\left(\frac{(u_\theta)_{\mathrm{th}}}{c_{\mathrm{th}}}\right)^2\right) A_{\mathrm{th}} \end{aligned} \tag{39}$$

where it is assumed that $(u_\theta/c_{\mathrm{th}})^2 << 1$. Using Eq. (39), one can find an approximation for the quasi-steady relative mass-flux variation:

$$\frac{\dot{m}_{\mathrm{st}} - \dot{m}^*}{\dot{m}^*} \equiv \frac{\delta\dot{m}_{\mathrm{st}}}{\dot{m}^*} \tag{40}$$

$$\simeq -\frac{1}{2}\left(\frac{(u_\theta)_{\mathrm{th}}}{c_{\mathrm{th}}}\right)^2. \tag{41}$$

Assuming a uniform circumferential velocity u_θ unifrom axial velocity u_{ax} and uniform density ρ, the swirl number defined by Gany et al. [13], becomes

$$\begin{aligned} S &= \frac{\int_0^R \rho u_{\mathrm{ax}} u_\theta r^2 \mathrm{d}r}{R\int_0^R \rho u_{\mathrm{ax}}^2 r\,\mathrm{d}r} \\ &= \frac{2u_\theta}{3u_{\mathrm{ax}}}. \end{aligned} \tag{42}$$

where $R = \sqrt{A/\pi}$. Solving for u_θ/u_{ax}, one finds

$$\frac{u_\theta}{u_{\mathrm{ax}}} = \frac{3}{2}S \tag{43}$$

Eq. (41), becomes

$$\frac{\delta\dot{m}_{\mathrm{st}}}{\dot{m}^*} \simeq -\frac{9}{8}S_{\mathrm{th}}^2. \tag{44}$$

In the upstream section with cross-sectional surface A_1, one finds, in terms of $(u_\theta)_1$ at A_1, using the conservation of angular momentum

$$\frac{\delta\dot{m}_{\mathrm{st}}}{\dot{m}^*} = -\frac{1}{2}\left(\frac{(u_\theta)_1}{c_{\mathrm{th}}}\right)^2 \frac{A_1}{A_{\mathrm{th}}} \tag{45}$$

After some Algebra and assuming a low upstream Mach number $M_1 << 1$, Eq. (45) becomes

$$\frac{\delta\dot{m}_{\mathrm{st}}}{\dot{m}^*} = -\frac{9}{8}S_1^2 \frac{A_{\mathrm{th}}}{A_1}\left(\frac{2}{\gamma+1}\right)^{\frac{2}{\gamma-1}}. \tag{46}$$

C. Influence of the Normal Shock

In the diverging part of the nozzle there is a normal shock in which the flow adapts from a supersonic state of density and pressure (ρ_v, p_v) at $M_v > 1$ upstream to a downstream subsonic state (ρ_h, p_h) at $M_h < 1$. The states are related by the integral mass, momentum and energy conservation laws. Assuming that the states are uniform yields the Rankine-Hugoniot shock relations. For an ideal gas with constant specific heats, these are[16]

$$\frac{p_h}{p_v} = 1 + \frac{2\gamma}{\gamma+1}\left(M_v^2 - 1\right) \tag{47}$$

$$\frac{\rho_v}{\rho_h} = 1 + \frac{2}{\gamma+1}\frac{1 - M_v^2}{M_v^2} \tag{48}$$

$\gamma \equiv c_p/c_v$ is the specific heat ratio (for air at room temperature $\gamma = 7/5$). By combining the first and second laws of Thermodynamics, one has

$$T\mathrm{d}s = \mathrm{d}e + p\mathrm{d}\rho^{-1} \tag{49}$$

where s is the specific entropy, T the absolute temperature and e the specific internal energy. By definition (for an ideal gas) $\mathrm{d}e = c_v\mathrm{d}T$ and $p = \rho RT$, with c_v the specific heat at constant volume and $R = c_v(\gamma - 1)$ the specific gas constant. Substitution in Eq. (49) yields

$$\frac{\mathrm{d}s}{c_v} = \frac{\mathrm{d}T}{T} + (\gamma - 1)\rho\mathrm{d}\rho^{-1} \tag{50}$$

which after integration becomes

$$\frac{s_h - s_v}{c_v} = \ln\left(\frac{T_h}{T_v}\right) - (\gamma - 1)\ln\left(\frac{\rho_h}{\rho_v}\right) \tag{51}$$

$$= \ln\left(\frac{p_h}{p_v}\right) - \gamma\ln\left(\frac{\rho_h}{\rho_v}\right). \tag{52}$$

Numerical results for the flow reported in Ref. [8], which are for the same stationary base flow condition as Kings' and Bake's experiments [5], indicate that $M_v \simeq 1.3$. Using this value of M_v, one finds for the increase in entropy across the shock

$$\frac{s_h - s_v}{c_v} \simeq 9.8 \times 10^{-3}. \tag{53}$$

This implies that the shock compression in the experiments of Kings and Bake [5] is almost adiabatic and does not interfere significantly with the acoustic wave propagation. The effect of the shock is therefore neglected.

D. Settling Chamber Pressure Variation

During an experiment, the duration of which is the circumferential injection time $t_\theta = 0.1$ s, thermal boundary layer growth in the settling chamber will approximately be limited to

$$\delta_{\text{thermal}} \simeq 2\sqrt{\frac{\kappa}{\rho c_p}t_\theta} \simeq 3 \times 10^{-3}\ \text{m}$$

where in air $\kappa/(\rho c_p) = 2 \times 10^{-5}\ \text{m}^2 \cdot \text{s}^{-1}$. Thus, the variations in settling chamber pressure due to change in injected mass flux can be assumed to be isentropic. The pressure in the settling chamber p_0, is furthermore taken to be uniform. This is because the settling chamber dimensions are small compared to the distance traveled by acoustic waves during the injection time: $340\ \text{m} \cdot \text{s}^{-1} \times 0.1\ \text{s} \simeq 34$ m.

Assuming a perfect gas, one has relation between for an isentropic compression $\mathrm{d}p$ a change in density $\mathrm{d}\rho$:

$$\frac{\mathrm{d}\rho}{\rho} = \frac{1}{\gamma}\frac{\mathrm{d}p}{p} \tag{54}$$

where $\gamma \equiv c_p/c_v$ (ratio of heat capacity at constant pressure c_p and c_v). The upstream settling chamber has a volume $V_0 = 4.6\,\mathrm{l}$. This is significantly larger than the volume in the tube section upstream from the nozzle inlet, which for modeling purposes will be neglected here. The fluid in the upstream settling chamber has a density ρ_0 and pressure p_0. For the (ideal) gas considered, the speed of sound in the reservoir is

$$c_0 = \sqrt{\gamma R T_0} \tag{55}$$

$$= \sqrt{\gamma \frac{p_0}{\rho_0}} \tag{56}$$

Before the experiment starts, one has a steady flow condition. Due to conservation of mass, one knows that the mass flux injected upstream is equal to the mass flux through the choked nozzle throat $\dot{m}_0^* = 41\ \mathrm{kg \cdot h^{-1}}$.

Now consider, starting at $t = 0$, there is a change of density $\delta\rho_0$, in V_0 due to a circumferential injection of $\dot{m}_\theta = 3.7\ \mathrm{kg \cdot h^{-1}}$ (estimated using a Swirl number of 0.826). A mass balance, assuming a choked nozzle flow, yields

$$\begin{aligned} V_0 \frac{\mathrm{d}\delta\rho_0}{\mathrm{d}t} &= \frac{V_0}{c_0^2}\frac{\mathrm{d}\delta p_0}{\mathrm{d}t} \\ &= \dot{m}_\theta - \delta\dot{m}_{\mathrm{vortex}} - \delta m^* \\ &\simeq \dot{m}_\theta - \delta\dot{m}_{\mathrm{vortex}} - \left(\frac{\delta m_0^*}{\dot{m}_0^*}\right)\dot{m}_0^* \end{aligned} \tag{57}$$

where $\dot{m}_0^*$ is the nozzle flow for the prevailing reservoir conditions (p_0, ρ_0) in the absence of a vortex. The term $\delta\dot{m}_{\mathrm{vortex}}$ is the reduction of mass flow through the nozzle due to the passage of the longitudinally vortex component.

Supposing a quasi one-dimensional and quasi-steady flow, for the critical mass flux through the nozzle throat $\dot{m}_0^*$, one has

$$\begin{aligned} \dot{m}_0^* &= A^* \rho^* c^* \\ &= A^* \rho_0 c_0 \left(\frac{2}{\gamma+1}\right)^{\frac{\gamma+1}{2(\gamma-1)}} \end{aligned} \tag{58}$$

where $A*$ is the cross-sectional surface of the critical nozzle throat. Using Eq. (58), and after some algebra, one finds

$$\begin{aligned} \frac{\delta\dot{m}_0^*}{\dot{m}_0^*} &= \frac{\delta\rho_0}{\rho_0} + \frac{\delta c_0}{c_0} \\ &= \left(\frac{\gamma+1}{2\gamma}\right)\frac{\delta p_0}{p_0} \end{aligned} \tag{59}$$

After substitution into Eq. (57) and some algebra, one finds the follwoing first order ordinary differential equation for δp_0:

$$\tau_0 \frac{\mathrm{d}\delta p_0}{\mathrm{d}t} = \frac{2\gamma p_0}{\gamma+1}\left(\frac{\dot{m}_\theta - \delta\dot{m}_{\mathrm{vortex}}}{\dot{m}_0^*}\right) - \delta p_0 \tag{60}$$

where

$$\tau_0 \equiv \frac{2\gamma\rho_0 V_0}{(\gamma+1)\dot{m}_0^*} \tag{61}$$

Assuming δp_0 remains small, one takes the coefficients in the Eq. (60) to be constants (linear approximation). The solution to Eq. (60) then is

$$\delta p_0 = \frac{2\gamma p_0}{\gamma+1}\left(\frac{\dot{m}_\theta - \delta\dot{m}_{\mathrm{vortex}}}{\dot{m}_0^*}\right)\left(1 - \exp\left(-\frac{t}{\tau_0}\right)\right). \tag{62}$$

Multiplying by $(\gamma+1)/(2\gamma p_0)$, one finds by virtue of Eq. (59):

$$\frac{\delta\dot{m}_0^*}{\dot{m}_0^*} = \frac{\dot{m}_\theta - \delta\dot{m}_{\text{vortex}}}{\dot{m}_0^*}\left(1-\exp\left(-\frac{t}{\tau_0}\right)\right) \tag{63}$$

$$\frac{\delta\dot{m}_0^*}{\dot{m}_0^*} \simeq \frac{\dot{m}_\theta - \delta\dot{m}_{\text{vortex}}}{\dot{m}_0^*}\left(\frac{t}{\tau_0}\right). \tag{64}$$

For an infinitely long tube, the change in mass flux δm_0^* caused by a variation of settling chamber pressure δp_0, will result in a plane pressure wave $\delta p_2'$ traveling downstream from the nozzle, given by

$$\delta p_2' = \rho_2 c_2 \delta u_2' \tag{65}$$

$$= \rho_2 c_2 \frac{\delta\dot{m}_0^*}{\dot{m}_0^*}\frac{\dot{m}_0^*}{\rho_2 A_2}. \tag{66}$$

Taking $(\delta p_2')_{\text{vortex}} \simeq -60$ Pa (from Fig. 3 experiments reported in Ref. [5]), one can estimate $\delta\dot{m}_{\text{vortex}}^*/\dot{m}_0^*$, as follows

$$\frac{\delta\dot{m}_{\text{vortex}}^*}{\dot{m}_0^*} \simeq -1.9\times10^{-2} \tag{67}$$

One estimates the circumferential mass-flux injection rate to be $\dot{m}_\theta = 3.7\ \text{kg}\cdot\text{h}^{-1}$, i.e., one has

$$\frac{\dot{m}_\theta}{\dot{m}_0^*} = \frac{3.7}{41}.$$

Using the estimation for $\delta\dot{m}_{\text{vortex}}/\dot{m}_0^*$ and $\dot{m}_\theta/\dot{m}_0^*$, one finds

$$\frac{\dot{m}_\theta - \delta\dot{m}_{\text{vortex}}}{\dot{m}_0^*} \simeq 0.109.$$

Eq. (64), becomes

$$\frac{\delta\dot{m}_0^*}{\dot{m}_0^*} \simeq 0.109\frac{t}{\tau_0} \tag{68}$$

As shown by Leyko et al. [14] the reflection of acoustic waves at the open downstream pipe termination limits the rising time of the pressure p_2' . The travel time along the pipe is of the order of $\tau_{\text{travel}} \simeq 6\text{m}/(340\text{m}\cdot\text{s}^{-1}) \simeq 0.02s$. Using Eq. 61, to estimate τ_0, yields $\tau_0 \simeq 0.6$ s. Now using Eq. (68) with $t = 0.02$ s and using Eq. (66), one can estimate $\delta p_2'$ due to the change in settling chamber conditions as:

$$\delta p_2' = \frac{\delta\dot{m}_0^*}{\dot{m}_0^*}\frac{c_2\dot{m}_0^*}{A_2} \simeq 11\ \text{Pa} \tag{69}$$

I.e. for an infinite pipe, the change in downstream acoustic pressure due to varied reservoir conditions would be approximately linear, and reach 11 Pa in 0.02 s. At microphones 3 and 4 (Fig. 7 in Ref. [5]) one observes an approximate 10 Pa global increase of p_2' at the end of the experiment.

Kings [12] also reports radial injection experiments, viz., in which the radial port in Fig. 2 was used for injection. In Fig. 11, results for apparent average radial injection mass-flow rates $0.55\ \text{kg}\cdot\text{h}^{-1}$ (blue line) and $1.10\ \text{kg}\cdot\text{h}^{-1}$ (red line) are shown. One notices that the resulting acoustic signal does not display the negative peak and positive peaks associated with the opening and closing of the valve in the circumferential injection experiments (see e.g. Figs. 3 and 4). However, one does observe a shifting of the pressure in the positive direction after radial injection has started (vertical dashed line at 0.1 s in Fig. 11) and negative direction after the valve was closed (vertical dashed line at 0.2 s in Fig. 11). Focusing on the red line which corresponds to an apparent average radial injection rate $1.10\ \text{kg}\cdot\text{h}^{-1}$, one sees shifts of ca. 10 Pa and −10 Pa (both pressure shifts are highlighted with black horizontal dashed dot dotted line) after the valve was opened and closed, respectively. Assuming that the apparent average injection mass flow rates are the same in the radial and circumferential experiments, one concludes that these pressure shifts are in part likely due to the pressure variation of the settling chamber described above. Note that the acoustic signal due to the increase in reservoir pressure is roughly linear in time. However, Fig. 11 displays a small abrupt increase of the measured acoustic signal. This might be due to some entropy effects. These are discussed in appendix E.

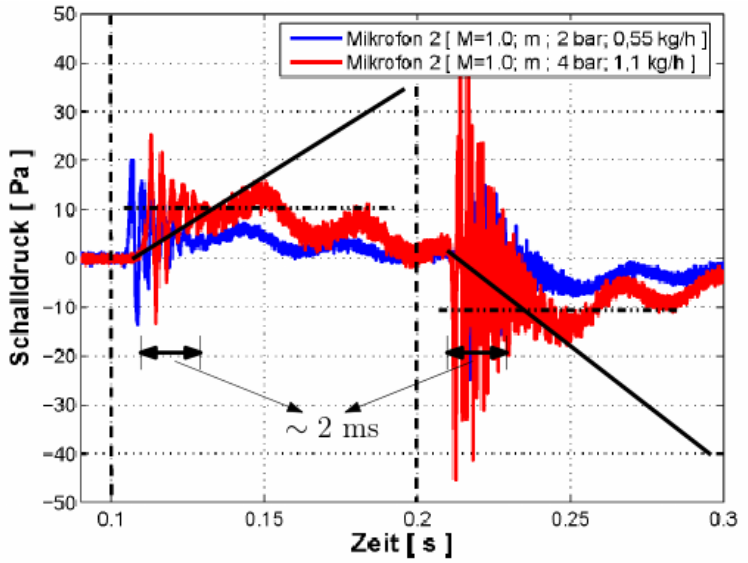

Fig. 11 Direct noise measurements obtained through radial gas injection. Straight black lines correspond to the predicted acoustic pressure signal generated by the change in reservoir pressure when the downstream tube is assumed to be perfectly anechoic. Figure taken from Ref. [12].

E. Influence of Entropy on the Sound Generated by Vortex-Nozzle Interaction

In the Entropy Wave Generator experiment reported by Bake et al. [8], a temperature perturbation of 10 K, which corresponds to $\Delta T/T_r \simeq 3.4 \times 10^{-2}$, was generated upstream from the nozzle on the same steady flow conditions as in Kings' and Bake's Vortex Wave Generator experiments [5]. Using a simple model, which assumes infinitely long downstream pipe, and uses the fact that for a choked nozzle the Mach number is fixed by the geometry,

$$\frac{u'}{u} = \frac{c'}{c}. \tag{70}$$

Assuming an ideal gas one has $c \propto \sqrt{T}$. Using Eq. (70) and solving for u', one finds

$$u' = \frac{\Delta T}{2T_r} u. \tag{71}$$

where the effect of the normal shock downstream from the nozzle throat on acoustics is neglected (see appendix C). The passage of an entropy perturbation through the nozzle throat is estimated to produce a downstream traveling pressure wave of magnitude:

$$\begin{aligned} p_2' &= \rho_2 c_2 u_2' \\ &\simeq \rho_2 c_2 \frac{\Delta T}{2T_r} u_2 \simeq 51 \text{ Pa}, \end{aligned} \tag{72}$$

where $u_2 \simeq u_1 (R_1/R_2)^2$ was used. The estimate of p_2' is about twice the maximum of the pressure perturbation observed by Bake et al. [8]. However, as noted by Leyko et al. [14] the predicted pressure is not reached, because an expansion wave, reflected at the downstream open pipe termination of the setup, arrives at the pressure probe before the temperature perturbation in the downstream pipe can reach its maximum predicted value. The propagation of acoustic waves in the downstream pipe results in a strongly damped quarter wavelength (open-closed pipe) oscillation in the downstream pipe sections of the experimental setup.

The maximum value predicted by numerical flow simulations for an infintely long downstream pipe by Leyko et al. [14] agree with the result of the proposed model (Eq. (72)).

While the main axial flow has a very low Mach number $M = 0.036$, the circumferential injected flow will have a much higher Mach number of typically $M_\theta = 0.3$. However, the injected mass is only about 10% of the total mass flux.

The fluid injected circumferentially travels through a long thin tube of 4 mm diameter with a typical flow velocity of 70 m $\cdot$ s^{-1}, corresponding to a Mach number M=0.2. This corresponds with a Reynolds number of 3×10^4, implying a turbulent flow in the injection needle. It seems reasonable to assume that at the injection point this gas will have reached a static temperature equal to the wall temperature of about $T = 293$ K. This implies that this fluid will have a total temperature of $T_r = T(1 + (\gamma - 1)M^2/2) = 295.3$ K. This circumferential injected mass flow will mix with the 10 times larger axial flow, which result in an increase of temperature of the order of 0.23 K. Using the model proposed above one finds an increase of the pressure p_2' of about 1 Pa:

$$p_2' \leq \frac{\Delta T}{2T_r} \rho_2 c_2 u_2 \simeq 1 \text{ Pa}. \tag{73}$$

This is negligible, compared to the magnitude of pressure waves generated by the axially-oriented component of the swirling flow structure [5] ($O\left(10^2 \text{ Pa}\right)$).

Acknowledgements

This work was carried out while Dr. Lionel Hirschberg was the beneficiary of a DLR-DAAD postdoctoral fellowship (no. 57424730). The authors thank Nancy Kings for the use of experimental data from her diploma thesis.

References

[1] Dotson, K. W., Koshigoe, S. and Pace, K. K., "Vortex Shedding in a Large Solid Rocket Motor Without Inhibitors at the Segmented Interfaces," *Journal of Propulsion and Power*, Vol. 13, No. 2, 1997, pp. 197–206 doi: 10.2514/2.5170

[2] Anthoine, J., "Experimental and Numerical Study of Aeroacoustic Phenomena in Large Solid Propellant Boosters, with application to the Ariane 5 solid rocket motor," PhD thesis, Université Libre de Bruxelles, Belgium, 2000

[3] Hirschberg, L., Schuller, T., Collinet, J., Schram, C. , and Hirschberg, A., "Analytical model for the prediction of pulsations in a cold-gas scale-model of a Solid Rocket Motor," *Journal of Sound and Vibration*, Vol. 19, April 2018, pp. 445–368 doi: 10.1016/j.jsv.2018.01.025

[4] Hirschberg, L., "Low order modeling of vortex driven self-sustained pressure pulsations in solid rocket motors," Ph.D. thesis, von Kármán Institute for Fluid Dynamics, Belgium, 2019

[5] Kings, N., and Bake, F., "Indirect combustion noise: noise generation by accelerated vorticity in a nozzle flow," *International Journal of Spray and Combustion Dynamics*, Vol. 2, No. 3, 2010, pp. 253–266 doi: 10.1260/1756-8277.2.3.253

[6] Ullrich, W. C., Bake, F., Kings, N., and Sattelmayer, T., "Numerical Investigations of Indirect Noise Generation by Accelerated Vorticity," *21st AIAA/CEAS Aeroacoustics Conference*, AIAA paper 2015-2382, June 2015 doi: 10.2514/6.2015-2382

[7] Howe, M. S., and Liu, J. T. C., "The Generation of Sound by Vorticity Waves in Swirling Duct Flows," *Journal of Fluid Mechanics*, Vol. 81, No. 2, June 1977, pp. 369–383 doi: 10.1017/S0022112077002109

[8] Bake, F., Richter, C., Mühlbauer, B., Kings, N., Röhle, I., Thiele, F., and Noll, B., "The Entropy Wave Generator (EWG): A reference case on entropy noise," *Journal of Sound and Vibration*, Vol. 326, No. 3-5, 2009, pp. 574–598 doi: 10.1016/j.jsv.2009.05.018

[9] Prandtl, L., "Strömungslehre," 3rd ed. ,Friedr. Vieweg & Sohn, Braunschweig, Germany, 1942

[10] Hulshoff, S. J., Hirschberg, A., and Hofmans, G. C. J., "Sound production of vortex nozzle interactions," *Journal of Fluid Mechanics*, Vol. 439, July 2001, pp. 335–352 doi: 10.1017/S0022112001004554

[11] Hirschberg, L., Hulshoff, S. J., Collinet, J., Schram, C., and Schuller, T., "Vortex nozzle interaction in solid rocket motors: A scaling law for upstream acoustic response," *The Journal of the Acoustical Society of America*, Vol. 144, No. 1, 2018, pp. EL46–EL51 doi: 10.1121/1.5046441

[12] Kings, N., "Schallentstehung durch beschleunigte Wirbelstärke in einer Düsenströmung," Diplomarbeit, Technischen Universität Berlin, Germany, 2009

[13] Gany, A., Mor, M., and Goldman, C., "Analysis and Characteristics of Choked Swirling Nozzle Flows," *AIAA Journal*, Vol. 43, No. 10, October 2005, pp. 2177–2181 doi: 10.2514/1.16887

[14] Leyko, M., Moreau, S., Nicoud, F., and Poinsot, T., "Numerical and analytical modelling of entropy noise in a supersonic nozzle with a shock," *Journal of Sound and Vibration*, Vol. 330, No. 16, August 2011, pp. 3944–3958 doi: 10.1016/j.jsv.2011.01.025

[15] van Holten, T., Heiligers, M., and Jaeken, A., "Choking Phenomena in a Vortex Flow Passing a Laval Tube: An Analytical Treatment," *Journal of Fluids Engineering*, Vol. 131, No. 041201, April 2009, pp. 1–7 doi: 10.1115/1.3089532

[16] Shapiro, A. H., "The Dynamics and Thermodynamics of compressible Fluid Flow: Vol. 1 and 2," 1st ed., The Ronald Press Company, New York, USA, 1953

[17] Gillespie, T. D., and Shearer, J. L., "The Control of Thrust and Flow Rate in Choked Nozzles by Vortex Generation," *Fluidics Quarterly*, 1972, pp. 50–55.

[18] Schlichting, H., "Boundary-Layer Theory," 7th ed. ,McGraw-Hill, New York, USA, 1979

[19] Dutton, J. C., "Swirling Supersonic Flow," *Journal of Propulsion and Power*, Vol. 3, No. 4, July 1987, pp. 342–349 doi: 10.2514/3.22996

[20] Dutton, J. C., "Correlation of Nozzle Performance Degradation Due to Swirl," *Journal of Propulsion and Power*, Vol. 5, No. 1, January 1989, pp. 126–128 doi: 10.2514/3.23125

[21] Yoo, S.-Y., Yoon, K.-Y., and Park, K.-A., "Influence of Swirl on the Discharge Coefficients of Sonic Nozzles," *KSME International Journal*, Vol. 11, No. 5, September 1997, pp. 574–581.

[22] Chang, F., and Dhir, V.-K., "Turbulent flow field in tangentially injected swirl flows in tubes," *International Journal Heat and Fluid Flow*, Vol. 15, No. 5, October 1994, pp. 346–356.

[23] Thompson, P. A., "Compressible-Fluid Dynamics," McGraw-Hill, New York, USA, 1972

[24] Steenbergen, W., and Voskamp, J., "The rate of decay of swirl in turbulent pipe flow," *Flow Measurement and Instrumentation*, Vol. 9, No. 2, June 1998, pp. 67–78.

[25] Neuhaus, D., and Röhle, I., "Schnellschaltende Ventile für Anwendungen in der Luft und Raumfahrt," *Deutscher Luft- und Raumfahrtkongress*, November 2006

[26] Billant, P., Chomaz, J.-M., and Huerre, P., "Experimental Study of Vortex Breakdown in Swirling Jets," *Journal of Fluid Mechanics*, Vol. 376, July 1998, pp. 183–219 doi: 10.1017/S0022112098002870

[27] Liang, H., and Maxworthy, T., "An Experimental Investigation of Swirling Jets," *Journal of Fluid Mechanics*, Vol. 525, September 2005, pp. 115–159 doi: 10.1017/S0022112004002629